Published in final edited form as:

Magn Reson Imaging. 2013 July ; 31(6): 840–846. doi:10.1016/j.mri.2013.02.008.

Non-Gaussian diffusion MRI assessment of brain microstructure in mild cognitive impairment and Alzheimer's disease☆

Maria F. Falangola[a,b,c,*], **Jens H. Jensen**[a,b], **Ali Tabesh**[a,b], **Caixia Hu**[d], **Rachael L. Deardorff**[a,b], **James S. Babb**[e], **Steven Ferris**[f], and **Joseph A. Helpern**[a,b,c]

[a]Department of Radiology and Radiological Science, Medical University of South Carolina, Charleston, SC 29425, USA

[b]Center for Biomedical Imaging, Medical University of South Carolina, Charleston, SC 29425, USA

[c]Department of Neuroscience Medical University of South Carolina, Charleston, SC 29425, USA

[d]The Nathan S. Kline Institute for Psychiatric Research, Orangeburg, NY 10962, USA

[e]Department of Radiology, New York University School of Medicine, New York, NY 10016, USA

[f]Alzheimer's Disease Center, Department of Psychiatry, New York University School of Medicine, New York, NY 10016, USA

Abstract

We report the first application of a novel diffusion-based MRI method, called diffusional kurtosis imaging (DKI), to investigate changes in brain tissue microstructure in patients with mild cognitive impairment (MCI) and AD and in cognitively intact controls. The subject groups were characterized and compared in terms of DKI-derived metrics for selected brain regions using analysis of covariance with a Tukey multiple comparison correction. Receiver operating characteristic (ROC) and binary logistic regression analyses were used to assess the utility of regional diffusion measures, alone and in combination, to discriminate each pair of subject groups. ROC analyses identified mean and radial kurtoses in the anterior corona radiata as the best individual discriminators of MCI from controls, with the measures having an area under the ROC curve (AUC) of 0.80 and 0.82, respectively. The next best discriminators of MCI from controls were diffusivity and kurtosis (both mean and radial) in the prefrontal white matter (WM), with each measure having an AUC between 0.77 and 0.79. Finally, the axial diffusivity in the hippocampus was the best overall discriminator of MCI from AD, having an AUC of 0.90. These preliminary results suggest that non-Gaussian diffusion MRI may be beneficial in the assessment of microstructural tissue damage at the early stage of MCI and may be useful in developing biomarkers for the clinical staging of AD.

☆This work was supported in part by research grants from the Werner Dannheisser Trust (JAH), the Litwin Fund for Alzheimer's Research (JAH), Institute for the Study of Aging (JAH), NIH Grant 1R01AG027852 (JAH) and NIH Grant P30 AG08051 (SHF).

*Corresponding author. Department of Radiology and Radiological Science, Center for Biomedical Imaging, MSC 120, Medical University of South Carolina, Charleston SC 29425-0120. Tel.: +1 843 876 2466; fax: +1 843 876 2469. falangol@musc.edu (M.F. Falangola).

Keywords

Alzheimer's disease; Mild cognitive impairment; MRI; Diffusion; Kurtosis; DKI

1. Introduction

Diffusion MRI imaging (dMRI) plays an important role in brain aging and dementia research due to its sensitivity to tissue microstructure. In mild cognitive impairment (MCI) and Alzheimer's disease (AD), diffusion tensor imaging (DTI) has become an important tool in the study of white matter (WM) alterations associated with disease status and progression. To date, most studies have focused on the diffusion metrics of fractional anisotropy (FA) and mean diffusivity (MD), but several recent studies have also employed measurements of axial and radial diffusivity, showing that these parameters may relate more closely to the underlying pathology and as such may be markers of disease progression [1–10]. Indeed, a recent meta-analysis [9] of case-controlled studies of DTI demonstrated an overall decrease of FA and increase of MD in AD and MCI groups compared with controls. Despite the large heterogeneity in the anatomy of the regions considered, these studies support the idea that dMRI is a potentially sensitive neuroimaging technique for the detection of WM changes in AD.

Even with these advances in characterizing WM changes with dMRI in normal aging, MCI and AD, it is well recognized that DTI yields only a fraction of the information potentially accessible by dMRI. This is mainly due to the fact that DTI is unable to quantify non-Gaussian diffusion [11]. In the brain, non-Gaussian diffusion is known to be substantial [12] and is believed to arise from diffusion barriers, such as cell membranes and organelles, as well as water-containing compartments (both extracellular and intracellular) with differing diffusion properties. Therefore, exploring non-Gaussian diffusion effects in AD could potentially provide a better understanding of microstructural tissue changes associated with disease pathology thereby improving our ability to evaluate disease progression.

Diffusional kurtosis imaging (DKI) is a minimal extension of DTI that enables the precise quantification of the diffusional kurtosis, a measure of diffusional non-Gaussianity, which naturally leads to metrics related to tissue microstructural complexity [13–16]. Aside from providing all of the diffusion indices conventionally obtained with DTI, DKI also provides the non-Gaussian metrics of mean kurtosis (MK) and axial ($K_{\parallel}$) and radial ($K_{\perp}$) kurtosis. These additional metrics can further help in our understanding of tissue microstructure. In addition, it has been shown that the extra information provided by DKI can be used to resolve intravoxel fiber crossings [15, 16], which is not possible with DTI. Although a relatively new method, DKI is already yielding promising preliminary results for several brain diseases including stroke [17–19], brain cancer [20,21], attention-deficit hyperactivity disorder [22], traumatic brain injury [23,24], Huntington's disease [25], epilepsy [26], as well as normal aging [27].

This is the first study to investigate brain tissue microstructural integrity using DKI in a cross-sectional investigation of both MCI and AD patients and in cognitively intact elderly controls. Our hypothesis is that the kurtosis metrics may contribute additional information

about brain tissue microstructure beyond that provided by conventional DTI parameters (i.e., FA and MD) and that this additional information may ultimately improve the characterization of the brain tissue microstructural changes occurring prior to the onset of clinically relevant cognitive deficits and cerebral atrophy.

2. Methods

2.1. Subjects

The protocol was approved by the Institutional Review Board of New York University (NYU) School of Medicine and all subjects gave written informed consent before participating in the study. All subjects were recruited from the Clinical Core of the NYU Alzheimer's disease Center. The control group (n = 16) fulfilled the following criteria: a) no evidence for dementia or MCI and b) a Global Deterioration Scale (GDS) = 1–2 [28]. The MCI group (n = 13) were defined as: a) mild memory impairment reported by the subject and/or a reliable informant, b) objective evidence of memory impairment, based on performance one standard deviation (SD) below the mean for age on Logical Memory II of the Wechsler Memory Scale [29], c) GDS = 3 (mild impairment), and d) insufficient cognitive and functional impairment for a diagnosis of dementia. For the AD group (n = 13), the diagnosis of probable AD was based on the criteria of Diagnostic and Statistical Manual of Mental Disorders, Fourth Edition (*DSM-IV*) [30] and the National Institute of Neurological and Communicative Diseases and Stroke/Alzheimer's Disease and Related Disorders Association (NINCDS/ADRDA) [31]. Additional inclusion criteria were GDS = 4–5 (moderate to moderately severe impairment, mild to moderate dementia) [28] and the absence of any medical, neurological, or psychiatric conditions that could account for the symptoms of dementia. The mean (+/− SD) GDS scores for the control, MCI and AD groups were 2.0 (+/− 0), 3.0 (+/− 0) and 4.4 (+/− 0.8), respectively (Table 1).

2.2. MRI

Images were acquired on a 3 Tesla Trio MR system (Siemens Medical Solutions, Erlangen, Germany). DKI experiments were performed using a twice-refocused spin-echo echo-planar imaging (EPI) diffusion sequence with a total of 30 different diffusion encoding directions. For each direction, six b-values (b = 0, 500, 1000, 1500, 2000, 2500 s/mm^2) were acquired. Other imaging parameters were: TR = 2300 ms, TE = 109 ms, FOV = 256 × 256 mm^2, matrix = 128 × 128, parallel imaging (GRAPPA) factor of 2, number of averages = 2, 15 oblique axial slices to cover the frontal and temporal regions, slice thickness = 2 mm, gap = 2 mm, voxel size = 2 × 2 × 2 mm^3. The scan duration for DKI was 11 min and 57 s. For anatomical reference and image segmentation, a 3D T1-weighted image was also acquired using a magnetization prepared rapid acquisition of gradient echoes (MPRAGE) sequence with the following parameters: TR = 2100 ms, TI = 1100 ms, shot spacing = 8.5 ms, TE = 3.9 ms, FOV = 256 × 192 mm^2, matrix = 256 × 192, parallel imaging factor of 2, 160 slices, slice thickness = 1 mm, scan duration = 3 min and 47 s. Additionally, we acquired a non-EPI T2-weighted image with the same matrix, slice location and thickness as for DKI but with a TE = 80 ms, which was used during the image registration process.

2.3. DKI post-processing

All raw diffusion images were inspected for bulk motion artifacts and corrupted images were excluded from post-processing. DKI post-processing was performed using in-house software based on methods previously published (http://www.nitrc.org/projects/dke) [32]. The software generates the parametric maps of mean diffusivity (MD), axial diffusivity ($D_{||}$), radial diffusivity ($D_{\perp}$), fractional anisotropy (FA), mean kurtosis (MK), axial kurtosis ($K_{||}$), and radial kurtosis ($K_{\perp}$). All of these are estimated from the diffusion and kurtosis tensors [32]. The MD corresponds to the diffusion coefficient averaged over all possible diffusion directions, whereas $D_{||}$ is the diffusion coefficient in the direction of the principal diffusion tensor eigenvector and $D_{\perp}$ is the diffusion coefficient averaged over all diffusion directions perpendicular to the principal diffusion tensor eigenvector. The additional diffusion metrics of MK, $K_{||}$ and $K_{\perp}$, are the kurtosis analogs of the MD, $D_{||}$ and $D_{\perp}$ [32] that quantify the diffusional non-Gaussianity. It is worth noting that, due to the inclusion of non-Gaussian effects, the DKI-derived estimates of the diffusion indices (MD, $D_{||}$ and $D_{\perp}$) will generally be more accurate than those obtained with conventional DTI [33]. For post-processing, diffusion-weighted images were spatially aligned with a 6-parameter rigid-body transformation to correct for head motion. Images were then spatially smoothed using a Gaussian filter with an in-plane full width at half maximum of 2.5 mm. Finally, the diffusivity and kurtosis parametric maps were generated by fitting the DKI model to the diffusion signal measurements [16,32] for each voxel.

2.4. Image analysis

Manually drawn and automatically generated regions-of-interest (ROIs) (Fig. 1) were used to compare the diffusion metrics between subject groups. Manual ROIs were created using MRIcron (http://www.mccauslandcenter.sc.edu/mricro/mricron). All registration and distortion correction steps were performed using Automatic Registration Toolbox (ART) [34]. Gray and white matter segmentation was performed using SPM5 (Wellcome Trust Centre for Neuroimaging, London, UK; http://www.fil.ion.ucl.ac.uk/spm). The prefrontal cortex, temporal lobe and hippocampus (H) ROIs were manually defined on the MPRAGE image of each subject following anatomical protocols reported in the literature [35–38]. The prefrontal cortex and temporal lobe ROIs were automatically segmented into white and gray matter compartments, and segmented prefrontal (sPF-WM) and temporal (sTMP-WM) WM ROIs were obtained. Additionally, localized prefrontal oval (PFo) and temporal oval (TMPo) WM ROIs were manually drawn on individual MPRAGE images. The hippocampus ROI was traced slice-by-slice using MRIcron, which allows for displaying each brain slice in three views (axial, sagittal and coronal), according to protocols reported in the literature [37,38], slightly modified. The coronal and sagittal views were used to define anterior, posterior, superior and inferior boundaries, respectively. The hippocampus ROI was defined with the following boundaries: a) the most anterior slice was limited by the uncal recessus of the temporal horn of the lateral ventricle and the amygdale, having the alveus as a landmark used for differentiation of the amygdala and hippocampus on the coronal plane; b) the posterior border of the hippocampus was defined as the slice before the complete disappearance of the hippocampal gray matter, which almost always was at the level where the splenium fused with the fornix. Additionally, the alveus was the superior border and the WM of the parahippocampal gyrus was the inferior border. ROIs for the genu of the corpus

callosum (gCC) and the anterior corona radiata (ACR) were drawn in the space of an MPRAGE template and were transformed back to the original MPRAGE coordinates of each subject for extraction of diffusion metrics. The MPRAGE template was created by spatially normalizing all MPRAGE images to the MPRAGE image of a healthy control with median cohort age, and averaging all normalized images. All ROIs (drawn in native or template space) were verified in native space by a neuropathologist (MFF) to ensure correct anatomical location and to avoid contamination of unintended tissue or cerebrospinal fluid (CSF). The volume of the hippocampus was determined from the manually drawn hippocampal ROI. The intracranial volume (ICV) was determined from the MPRAGE image after skull stripping with Brain Extraction Tool [39]. Hippocampal volumes are represented as a fraction of ICV (see Table 1). The diffusion parametric maps of each subject were spatially aligned to the subject's MPRAGE space using a nonlinear transformation between the subject's b = 0 and T2-weighted images combined with a rigid-body transformation between the subject's T2-weighted and MPRAGE images. Finally, the average regional diffusion values were obtained from the voxels within each ROI. To minimize the effect of CSF contamination, all voxels with MD > 2 μm^2/ms were excluded from the ROIs before obtaining the diffusion values.

2.5. Statistical analysis

The subject groups were compared in terms of demographic factors (e.g., age, gender, education). Chi-square analysis was used for gender comparison, and Tukey post hoc corrected analysis of variance was used for age, education, GDS and MMSE scores and hippocampus volume. Analysis of covariance (ANCOVA) was used to compare subject groups in terms of each regional diffusion measure. A separate analysis was conducted for each measure within each region. In each case, the regional measure was the dependent variable and the model included age as a numeric factor and group membership as a classification factor. The error variance was allowed to differ across subject groups to avoid the unnecessary assumption of variance homogeneity. P-values for group comparisons were adjusted for multiple comparisons using a Tukey honestly significant difference correction. Receiver operating characteristic (ROC) and binary logistic regression analyses were used to assess the diagnostic utility of regional diffusion measures, alone and in combination, to discriminate each pair of subject groups. All reported p-values are two-sided with significance defined as $p < 0.05$. SAS 9.3 (SAS Institute, Cary, NC) was used for all computations.

3. Results

As shown in Table 1, there were no significant differences in age, gender or education level between all three patient groups. As expected, there were significant differences in GDS and MMSE scores for MCI and AD groups compared with control group. There was also a significant volume reduction in the hippocampus of the AD patients.

Fig. 2 shows the means (+/−SD) of the diffusivity metrics for the three groups (control, MCI and AD) for each ROI; it also indicates the indices that were found to be statistically significant after Tukey's multiple comparison correction. Relative to the control group, AD

patients showed significant mean, axial and radial diffusivity increases in all brain regions examined. No statistically significant fractional anisotropy differences were found in any of the ROIs, but AD patients showed a trend towards reduced fractional anisotropy in all white matter regions examined and in the hippocampus. When comparing AD and MCI groups, only in the hippocampus were the mean, axial and radial diffusivity values significantly increased. Relative to the control group, the MCI group showed significantly increased mean diffusivity in the PFo and radial diffusivity in the PFo and ACR.

Fig. 3 shows the means (+/− SD) of the kurtosis metrics for the three groups (control, MCI and AD) for each ROI, with the indices that were found to be statistically significant after Tukey's multiple comparison correction. Relative to the C group, AD patients showed significant mean kurtosis and radial kurtosis decrease in the ACR, TMPo, sTMP-WM and gCC. Radial kurtosis was also decreased in the sPF-WM; axial kurtosis was only decreased in the ACR. When comparing C and MCI groups, we observed decreased mean kurtosis and radial kurtosis in the PFo, and a decrease of all kurtosis metrics (MK, $K_{\parallel}$ and $K_{\perp}$) in the ACR.

ROC analysis identified axial diffusivity in the hippocampus as the best overall discriminator of AD from MCI with an area under the ROC curve (AUC) of 0.90. The logistic regression analysis failed to identify any set of two or more regional diffusion measures that were significant independent discriminators of MCI from AD. Additionally, ROC analyses (Table 2) identified mean and radial kurtosis in the ACR as the best individual discriminators of MCI from controls, with the measures having an AUC of 0.80 and 0.82, respectively. The ROC analysis identified mean kurtosis, radial kurtosis, mean diffusion and radial diffusion in the PFo region as the next best discriminators of MCI from controls, with each measure having an AUC between 0.77 to 0.78.

4. Discussion

Several studies have demonstrated regional increased rates of cerebral atrophy several years before elderly people reach the stage known as MCI [40,41]. While these observations are consistent with the presence of prodromal AD, the mechanism(s) responsible are still poorly understood. More important, the differentiation of normal elderly from patients with MCI appears to be the most challenging task. Very little has been published about the diagnostic utility of dMRI in distinguishing patients with MCI from cognitively normal subjects [42,43]. We hypothesize that alterations of brain tissue microstructure may be evident prior to the onset of cerebral atrophy and clinically relevant cognitive deficits. Our results provide evidence that diffusion differences, represented by significant changes in the mean, axial and radial kurtosis and radial diffusivity in the ACR and changes in the mean and radial kurtosis and mean and radial diffusivity in the PFo, are capable of discriminating controls from MCI patients, a stage where atrophy is not yet predominant. At this early stage, these diffusion differences may reflect fundamental alterations in myelin integrity, relatively independent of the Wallerian degeneration from neuronal loss that causes the neurodegenerative process, which is in accordance with the mechanism outlined by Bartzokis [44].

Interestingly, all diffusional kurtosis metrics from our data showed significant changes in the ACR, differentiating elderly controls from both MCI and AD. Radial diffusivity also showed significant changes in the ACR, but the kurtosis metrics were the best individual discriminators of controls from MCI. ACR is a major WM fiber bundle [45], and DTI studies have found that the WM integrity in the left ACR is associated with the executive function [46]. Additionally, DTI parameter changes in this WM tract have been described and associated with cognitive deficits, including impaired information processing speed [47] that occurs with aging and in vascular cognitive impairment [48,49]. To our knowledge, there are limited dMRI studies that have previously mentioned ACR as a WM tract affected in MCI and AD [7,50]. Additionally, in AD, the degree of atrophy in periventricular structures such as corona radiata is associated with cognitive impairment based on MMSE scores [51].

Previous studies utilizing DTI have reported brain tissue microstructural changes, predominantly WM damage, in AD and MCI subjects [3–10]. Our findings agree with these previous observations demonstrating significant increases in diffusivity in AD; these diffusivity changes have little anatomical specificity, and they are possibly related to the combination of axonal loss and myelin damage. In our study, however, axial diffusivity in the hippocampus was identified as the best overall discriminator of AD from MCI. This diffusivity change may be a more specific metric for disease progression representing axonal damage, or may potentially be a result of CSF partial volume in a region that presents with a severe degree of atrophy in AD patients. Indeed, our data did reveal a significant ($p < 0.05$) volume reduction in the hippocampus for AD relative to controls and MCI, but not for MCI relative to controls. In comparison to the diffusivities, the kurtosis metrics are less sensitive to CSF partial volume [52] and were not significantly different in the hippocampus for the MCI and AD groups.

It is noteworthy that, while our AD patients showed a trend towards reduced fractional anisotropy in all WM regions examined and in the hippocampus, we did not find significant differences in fractional anisotropy between the two groups as previously reported [4,5,10,51,53]. This may be due to the variance in mean fractional anisotropy across the control group, which is an age-related characteristic, methodological difference between DTI and DKI acquisition and processing parameters and/or the influence of partial volume effects mentioned above.

Finally, an important consideration for imaging studies of AD patients is the time necessary to acquire the data, which should be kept to a minimum. In this respect, DKI is currently the only method that allows for precise quantification of diffusional non-Gaussianity and that can be performed on any clinical MR system with scan duration on the order of several minutes. It should be noted that we have recently reported a whole-brain DKI acquisition protocol that can be performed in approximately 7 minutes [16].

The quantitative diffusion metrics derived from DKI may play an important role in assessing changes in WM characteristics commonly found in a range of neurodegenerative diseases. The present study demonstrates that these metrics may be an early marker of WM alterations during AD pathology progression.

5. Limitations

Some limitations of the present study should be noted. First, replication of the DKI method in a larger sample is needed. Second, this work was performed using an early version of our DKI protocol that did not cover the whole brain. Finally, due to our limited sample size, WM hyperintensities were not included as a covariant in our analysis.

6. Conclusion

In summary, the present study demonstrates, for the first time, the ability to characterize tissue microstructural changes in MCI and AD patients based upon the assessment of non-Gaussian brain water diffusion, and it suggests that kurtosis parameters are useful additions to other diffusion measurements that may help to establish reliable biomarkers for AD diagnosis and progression. The possibility of assessing the clinical status of subjects at a single point in time represents a promising approach toward developing an efficient method for earlier disease detection and differentiation throughout the progression of AD. Future longitudinal studies should examine whether DKI measures of WM integrity can effectively identify MCI patients at high risk of progressing to dementia.

Acknowledgments

The authors wish to acknowledge and thank Drs. Henry Rusinek, James B. Golomb and Stephen D. Ginsberg for their helpful discussions and input, Robyn Waters, Jane Kwon and Edgar Suan for patient coordination and Amanda Allen for technical assistance.

References

1. Assaf Y. Can we use diffusion MRI as a bio-marker of neurodegenerative processes? Bioessays. 2008; 30:1235–45. [PubMed: 18937377]
2. Madden DJ, Bennett IJ, Burzynska A, Potter GG, Chen NK, Song AW. Diffusion tensor imaging of cerebral white matter integrity in cognitive aging. Biochim Biophys Acta. 2012; 1822(3):386–400. [PubMed: 21871957]
3. Medina D, Toledo-Morrell L, Urresta F, Gabrieli JD, Moseley M, Fleischman D, et al. White matter changes in mild cognitive impairment and AD: a diffusion tensor imaging study. Neurobiol Aging. 2006; 27:663–72. [PubMed: 16005548]
4. Hess CP. Update on diffusion tensor imaging in Alzheimer's disease. Magn Reson Imaging Clin N Am. 2009; 17(2):215–24. [PubMed: 19406355]
5. Damoiseaux JS, Smith SM, Witter MP, Sanz-Arigita EJ, Barkhof F, Scheltens P, et al. White matter tract integrity in aging and Alzheimer's disease. Hum Brain Mapp. 2009; 30(4):1051–9. [PubMed: 18412132]
6. Pievani M, Agosta F, Pagani E, Canu E, Sala S, Absinta M, et al. Assessment of white matter tract damage in mild cognitive impairment and Alzheimer's disease. Hum Brain Mapp. 2010; 31(12): 1862–75. [PubMed: 20162601]
7. Canu E, McLaren DG, Fitzgerald ME, Bendlin BB, Zoccatelli G, Alessandrini F, et al. Microstructural diffusion changes are independent of macrostructural volume loss in moderate to severe Alzheimer's disease. J Alzheimers Dis. 2010; 19(3):963–76. [PubMed: 20157252]
8. Acosta-Cabronero J, Williams GB, Pengas G, Nestor PJ. Absolute diffusivities define the landscape of white matter degeneration in Alzheimer's disease. Brain. 2010; 133:529–39. [PubMed: 19914928]
9. Sexton CE, Kalu UG, Filippini N, Mackay CE, Ebmeier KP. A meta-analysis of diffusion tensor imaging in mild cognitive impairment and Alzheimer's disease. Neurobiol Aging. 2011; 32(12): 2322.e5–2322.e18.

10. Bosch B, Arenaza-Urquijo EM, Rami L, Sala-Llonch R, Junqué C, Solé-Padullés C, et al. Multiple DTI index analysis in normal aging, amnestic MCI and AD. Relationship with neuropsychological performance. Neurobiol Aging. 2012; 33(1):61–74. [PubMed: 20371138]
11. Alexander DC. Multiple-fiber reconstruction algorithms for diffusion MRI. Ann N Y Acad Sci. 2005; 1064:113–33. [PubMed: 16394152]
12. Le Bihan D. Molecular diffusion, tissue microdynamics and microstructure. NMR Biomed. 1995; 8(7–8):375–86. [PubMed: 8739274]
13. Jensen JH, Helpern JA, Ramani A, Lu H, Kaczynski K. Diffusional kurtosis imaging: the quantification of non-Gaussian water diffusion by means of magnetic resonance imaging. Magn Reson Med. 2005; 53(6):1432–40. [PubMed: 15906300]
14. Lu H, Jensen JH, Ramani A, Helpern JA. Three-dimensional characterization of non-Gaussian water diffusion in humans using diffusion kurtosis imaging. NMR Biomed. 2006; 19(2):236–47. [PubMed: 16521095]
15. Lazar M, Jensen JH, Xuan L, Helpern JA. Estimation of the orientation distribution function from diffusional kurtosis imaging. Magn Reson Med. 2008; 60(4):774–81. [PubMed: 18816827]
16. Jensen JH, Helpern JA. MRI quantification of non-Gaussian water diffusion by kurtosis analysis. NMR Biomed. 2010; 23(7):698–710. [PubMed: 20632416]
17. Jensen JH, Falangola MF, Hu C, Tabesh A, Rapalino O, Lo C, et al. Preliminary observations of increased diffusional kurtosis in human brain following recent cerebral infarction. NMR Biomed. 2011; 24(5):452–7. [PubMed: 20960579]
18. Fung SH, Roccatagliata L, Gonzalez RG, Schaefer PW. MR diffusion imaging in ischemic stroke. Neuroimaging Clin N Am. 2011; 21(2):345–77. [PubMed: 21640304]
19. Hui ES, Fieremans E, Jensen JH, Tabesh A, Feng W, Bonilha L, et al. Stroke assessment with diffusional kurtosis imaging. Stroke. 2012; 43(11):2968–73. [PubMed: 22933581]
20. Raab P, Hattingen E, Franz K, Zanella FE, Lanfermann H. Cerebral gliomas: diffusional kurtosis imaging analysis of microstructural differences. Radiology. 2010; 254(3):876–81. [PubMed: 20089718]
21. Van Cauter S, Veraart J, Sijbers J, Peeters RR, Himmelreich U, De Keyzer F, et al. Gliomas: diffusion kurtosis MR imaging in grading. Radiology. 2012; 263(2):492–501. [PubMed: 22403168]
22. Helpern JA, Adisetiyo V, Falangola MF, Hu C, Di Martino A, Williams K, et al. Preliminary evidence of altered gray and white matter microstructural development in the frontal lobe of adolescents with attention-deficit hyperactivity disorder: a diffusional kurtosis imaging study. J Magn Reson Imaging. 2011; 33(1):17–23. [PubMed: 21182116]
23. Zhuo J, Xu S, Porter J, Mullins RJ, Simon JZ, Fiskum G, et al. Diffusion kurtosis as an in vivo imaging marker for reactive astrogliosis in traumatic brain injury. Neuroimage. 2011; 59(1):467–77. [PubMed: 21835250]
24. Grossman EJ, Ge Y, Jensen JH, Babb JS, Miles L, Reaume J, et al. Thalamus and cognitive impairment in mild traumatic brain injury: a diffusional kurtosis imaging study. J Neurotrauma. 2011; 29(13):2318–27. [PubMed: 21639753]
25. Blockx I, Verhoye M, Van Audekerke J, Bergwerf I, Kane JX, Delgado Y, et al. Identification and characterization of huntington related pathology: an in vivo DKI imaging study. Neuroimage. 2012; 63(2):653–62. [PubMed: 22743196]
26. Gao Y, Zhang Y, Wong CS, Wu PM, Zhang Z, Gao J, et al. Diffusion abnormalities in temporal lobes of children with temporal lobe epilepsy: a preliminary diffusional kurtosis imaging study and comparison with diffusion tensor imaging. NMR Biomed. 2012; 25(12):1369–77. [PubMed: 22674871]
27. Falangola MF, Jensen JH, Babb JS, Hu C, Castellanos FX, Di Martino A, et al. Age-related non-Gaussian diffusion patterns in the prefrontal brain. J Magn Reson Imaging. 2008; 28(6):1345–50. [PubMed: 19025941]
28. Reisberg B, Borenstein J, Salob SP, Ferris SH, Franssen E, Georgotas A. Behavioral symptoms in Alzheimer's disease: phenomenology and treatment. J Clin Psychiatry. 1987; 48(Suppl):9–15.
29. Wechsler, D. Wechsler Memory Scale-Revised. San Antonio: Psychological Corporation/Harcourt Brace Javanovich; 1987.

30. American Psychiatric Association. DSM III-R: diagnostic and statistical manual of mental disorders. Washington, DC: 1987.
31. McKhann G, Drachman D, Folstein M, Katzman R, Price D, Stadlan EM. Clinical diagnosis of Alzheimer's disease: report of the NINCDS-ADRDA Work Group under the auspices of Department of Health and Human Services Task Force on Alzheimer's Disease. Neurology. 1984; 34(7):939–44. [PubMed: 6610841]
32. Tabesh A, Jensen JH, Ardekani BA, Helpern JA. Estimation of tensors and tensor-derived measures in diffusional kurtosis imaging. Magn Reson Med. 2011; 65(3):823–36. [PubMed: 21337412]
33. Veraart J, Poot DH, Van Hecke W, Blockx I, Van der Linden A, Verhoye M, et al. More accurate estimation of diffusion tensor parameters using diffusion Kurtosis imaging. Magn Reson Med. 2011; 65(1):138–45. [PubMed: 20878760]
34. Ardekani BA, Guckemus S, Bachman A, Hoptman MJ, Wojtaszek M, Nierenberg J. Quantitative comparison of algorithms for inter-subject registration of 3D volumetric brain MRI scans. J Neurosci Methods. 2005; 142(1):67–76. [PubMed: 15652618]
35. Crespo-Facorro B, Kim JJ, Andreasen NC, O'Leary DS, Wiser AK, Bailey JM, et al. Human frontal cortex: an MRI-based parcellation method. Neuroimage. 1999; 10(5):500–19. [PubMed: 10547328]
36. Kim JJ, Crespo-Facorro B, Andreasen NC, O'Leary DS, Zhang B, Harris G, et al. An MRI-based parcellation method for the temporal lobe. Neuroimage. 2000; 11(4):271–88. [PubMed: 10725184]
37. Tae WS, Kim SS, Lee KU, Nam EC, Kim KW. Validation of hippocampal volumes measured using a manual method and two automated methods (FreeSurfer and IBASPM) in chronic major depressive disorder. Neuroradiology. 2008; 50(7):569–81. [PubMed: 18414838]
38. Konrad C, Ukas T, Nebel C, Arolt V, Toga AW, Narr KL. Defining the human hippocampus in cerebral magnetic resonance images–an overview of current segmentation protocols. Neuroimage. 2009; 47(4):1185–95. [PubMed: 19447182]
39. Smith SM. Fast robust automated brain extraction. Hum Brain Mapp. 2002; 17(3):143–55. [PubMed: 12391568]
40. Rusinek H, De Santi S, Frid D, Tsui WH, Tarshish CY, Convit A, et al. Regional brain atrophy rate predicts future cognitive decline: 6-year longitudinal MR imaging study of normal aging. Radiology. 2003; 229(3):691–6. [PubMed: 14657306]
41. Jack CR Jr, Shiung MM, Weigand SD, O'Brien PC, Gunter JL, Boeve BF, et al. Brain atrophy rates predict subsequent clinical conversion in normal elderly and amnestic MCI. Neurology. 2005; 65(8):1227–31. [PubMed: 16247049]
42. Risacher SL, Shen L, West JD, Kim S, McDonald BC, Beckett LA, et al. Alzheimer's Disease neuroimaging initiative (ADNI). longitudinal MRI atrophy biomarkers: relationship to conversion in the ADNI cohort. Neurobiol Aging. 2010; 31(8):1401–18. [PubMed: 20620664]
43. Zhuang L, Wen W, Zhu W, Trollor J, Kochan N, Crawford J, et al. White matter integrity in mild cognitive impairment: a tract-based spatial statistics study. Neuroimage. 2010; 53(1):16–25. [PubMed: 20595067]
44. Bartzokis G. Age-related myelin breakdown: a developmental model of cognitive decline and Alzheimer's disease. Neurobiol Aging. 2004; 25:5–18. [PubMed: 14675724]
45. Wakana S, Jiang H, Nagae-Poetscher LM, van Zijl PC, Mori S. Fiber tract-based atlas of human white matter anatomy. Radiology. 2004; 230(1):77–87. [PubMed: 14645885]
46. Niogi S, Mukherjee P, Ghajar J, McCandliss BD. Individual differences in distinct components of attention are linked to anatomical variations in distinct white matter tracts. Front Neuroanat. 2010; 4:2. [PubMed: 20204143]
47. Duering M, Zieren N, Hervé D, Jouvent E, Reyes S, Peters N, et al. Strategic role of frontal white matter tracts in vascular cognitive impairment: a voxel-based lesion-symptom mapping study in CADASIL. Brain. 2011; 134(Pt 8):2366–75. [PubMed: 21764819]
48. Yin X, Han Y, Ge H, Xu W, Huang R, Zhang D, et al. Inferior frontal white matter asymmetry correlates with executive control of attention. Hum Brain Mapp. 2013; 34(4):796–813. [PubMed: 22110013]

49. Sasson E, Doniger GM, Pasternak O, Tarrasch R, Assaf Y. Structural correlates of cognitive domains in normal aging with diffusion tensor imaging. Brain Struct Funct. 217(2):503–15. 201. [PubMed: 21909706]

50. Canu E, McLaren DG, Fitzgerald ME, Bendlin BB, Zoccatelli G, Alessandrini F, et al. Mapping the structural brain changes in Alzheimer's disease: the independent contribution of two imaging modalities. J Alzheimers Dis. 2011; 26(3):263–74.

51. Ferrarini L, Palm WM, Olofsen H, van der Landen R, Jan Blauw G, Westendorp RG, et al. MMSE scores correlate with local ventricular enlargement in the spectrum from cognitively normal to Alzheimer disease. Neuroimage. 2008; 39(4):1832–8. [PubMed: 18160312]

52. Yang AW, Jensen JH, Hu CC, Tabesh A, Falangola MF, Helpern JA. Effect of cerebral spinal fluid suppression for diffusional kurtosis imaging. J Magn Reson Imaging. 2013; 37(2):365–71. [PubMed: 23034866]

53. Palesi F, Vitali P, Chiarati P, Castellazzi G, Caverzasi E, Pichiecchio A, et al. DTI and MR volumetry of hippocampus-PC/PCC circuit: in search of early micro- and macrostructural signs of Alzheimers's disease. Neurol Res Int. 2012:517876. Epub 2011 Jun 12. [PubMed: 21773026]

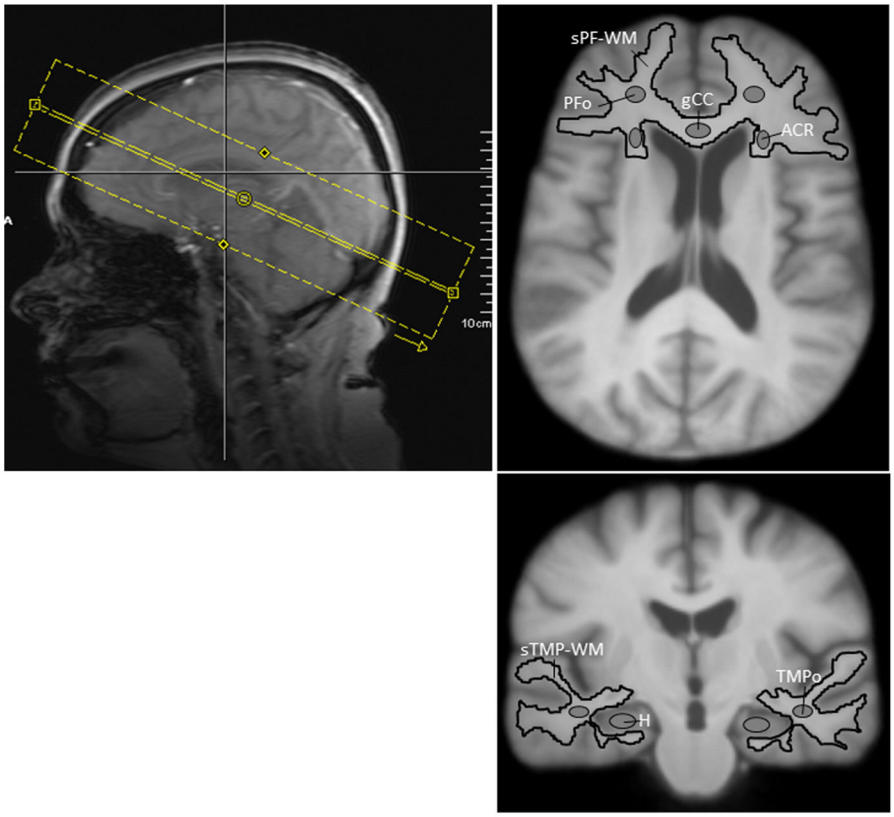

Fig. 1.

DKI acquisition slab and regions of interest (ROIs). ROIs: Segmented prefrontal white matter (sPF-WM); prefrontal oval (PFo); genu of the corpus callosum (gCC); anterior corona radiata (ACR); segmented temporal white matter (sTMP-WM); temporal oval (TMPo); hippocampus (H).

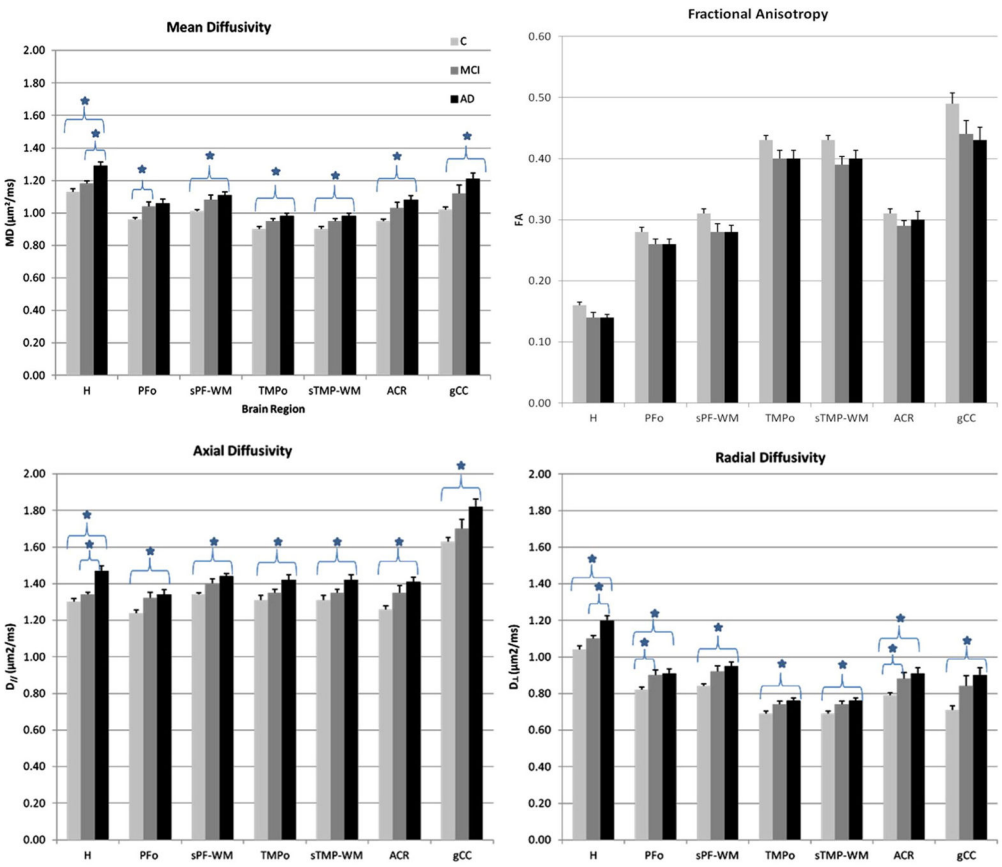

Fig. 2.

Means (+/− s.d.) for diffusivity metrics in each ROI, for each study group. Indices that were found to be statistically significant after Tukey's multiple comparison correction (significance defined as $p < 0.05$) are labeled with *. All diffusion coefficient metrics (MD, $D_{\parallel}$ and $D_{\perp}$) were statistically different between C and AD groups for all ROIs. No statistical significant FA differences for any ROIs. ROIs: segmented prefrontal white matter (sPF-WM); prefrontal oval (PFo); genu of the corpus callosum (gCC); anterior corona radiata (ACR); segmented temporal white matter (sTMP-WM); temporal oval (TMPo); hippocampus (H). C = Controls; MCI = mild cognitive impairment; AD = Alzheimer's disease.

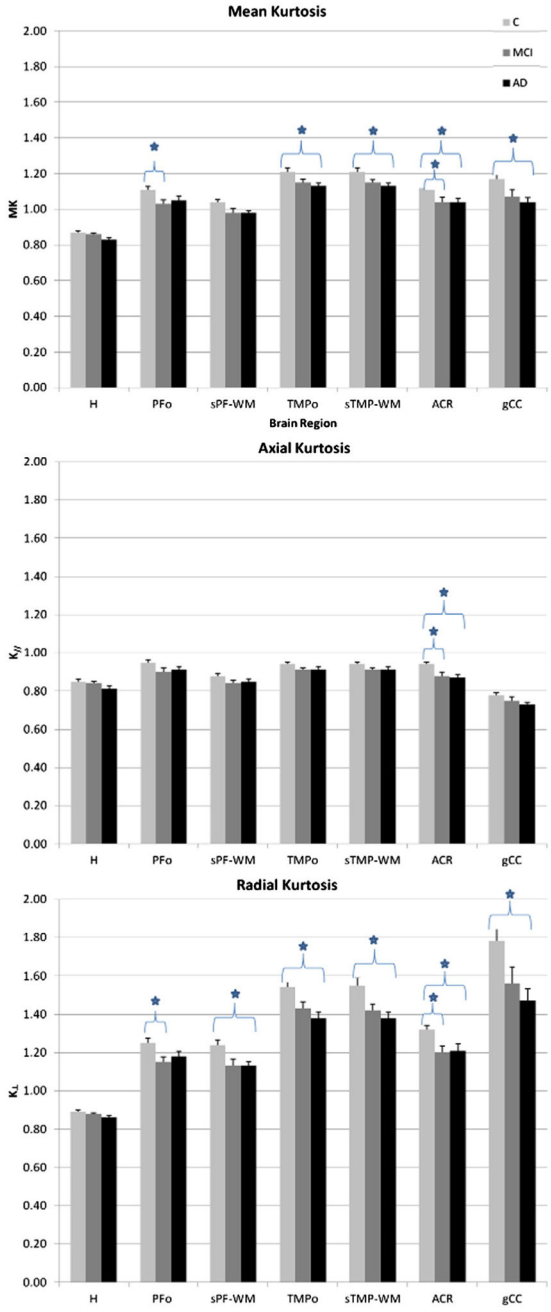

Fig. 3.

Means (+/− s.d.) for kurtosis metrics in each ROI, for each study group. Indices that were found to be statistically significant after Tukey's multiple comparison correction (significance defined as $p < 0.05$) are labeled with *. ROIs: segmented prefrontal white matter (sPF-WM); prefrontal oval (PFo); genu of the corpus callosum (gCC); anterior corona radiata (ACR); segmented temporal white matter (sTMP-WM); temporal oval (TMPo); hippocampus (H). C = controls; MCI = mild cognitive impairment; AD = Alzheimer's disease.

Table 1

Demographic and hippocampus volume summary.

	C (n = 16)	MCI (n = 13)	AD (n = 13)
Age (years)	71.6 ± 7.6	73.5 ± 10.0	75.0 ± 7.4
Gender (male/female)	5/11	8/5	5/8
Education (years)	16.4 ± 2.6	16.8 ± 2.2	16.4 ± 2.6
GDS	2 ± 0	3 ± 0&	4.4 ± 0.8&**
MMSE	29.6 ± 0.8	28.8 ± 1.5	19.8 ± 7.3&**
Hippocampus volume (fraction of ICV)	0.30 ± 0.06	0.31 ± 0.07	0.24 ± 0.05&**

Mean ± standard deviation; C = controls; MCI = mild cognitive impairment; AD = Alzheimer's disease; GDS = geriatric depression scale; MMSE = mini mental state exam; ICV = Intracranial volume. Significantly different (&$p < 0.001$ vs. C), (**$p < 0.001$ vs. MCI).

Table 2

Area under the receiver operating characteristic curve (AUC) for discrimination of patients with mild cognitive impairment (MCI) from controls (C).

Region	Metric	AUC	P-value
ACR	MK	0.80	0.035
ACR	$K_{\perp}$	0.82	0.027
PFo	MD	0.77	0.044
PFo	$D_{\perp}$	0.74	0.050
PFo	MK	0.78	0.039
PFo	K	0.78	0.037

Metrics: MD = mean diffusion; $D_{\perp}$ = radial diffusion; MK = mean kurtosis; $K_{\perp}$ = radial kurtosis; ROIs: anterior corona radiata (ACR); prefrontal oval (PFo). AUC (area under the curve).